Ab initio calculations of two-photon absorption spectra in semiconductors

Misao Murayama and Takashi Nakayama
Department of Physics, Faculty of Science, Chiba University, Yayoi Inage, Chiba 263, Japan
(Received 22 February 1995; revised manuscript received 5 May 1995)

Degenerate and nondegenerate two-photon absorption spectra and their anisotropy are evaluated for various semiconductors, by using *ab initio* full-band-structure and microscopic-nonlinear-susceptibility calculations. It is shown that most semiconductors have abundant spectral structures originating from the critical-point transitions similar to one-photon absorption. The calculated spectra are in good agreement with recent accurate experimental results, demonstrating the usefulness of *ab initio* approach in the two-photon-absorption calculations.

I. INTRODUCTION

Two-photon absorption (TPA) is a powerful tool to study the optical and electronic properties of materials. Because TPA follows the unique selection rules, TPA provides complementary material information to the one-photon absorption (OPA).[1,2] On the other hand, in the application field, TPA plays a crucial role in limiting the optical transparency of materials and in causing laser-induced damage to compounds.[3] It has also been recognized that nonlinear refraction can be related to TPA through a nonlinear Kramers-Krönig transformation.[4,5]

Although a number of experiments have been carried out to evaluate TPA spectra of various materials,[3] the measurements were limited to particular photon energies and the determination of TPA magnitude and anisotropy was difficult due to its sensitivity to experimental variables,[3] such as laser-pulse duration, peak power, laser coherence, and the presence of free carriers. However, the recent developments of laser equipment and the superior experimental method such as "Z-scan" and "two-beam coupling" have eliminated these disadvantages,[6] thus enabling the precise measurement of TPA in a wide photon-energy range.

From the theoretical viewpoint, numerous model-band calculations of TPA spectra have been performed,[3] whose results strongly depend on band parameters adopted. The two-parabolic-band model by Wherrett[7] provides the proper scaling of TPA with material parameters and photon energy. The TPA calculational scheme based on the Kane band-structure model by Hutchings and Van Stryland[8] explains well the recent experimental data of various zinc-blende semiconductors. Recently, Hutchings and Wherrett[9] have calculated TPA anisotropy of GaAs and InSb using the Luttinger-Kohn band-structure model. However, these calculations are limited to the TPA around the center of the Brillouin zone of direct-gap materials having the zinc-blende structure, where the band parameters are well known. In order to evaluate the TPA spectra of materials having transitions at the Brillouin-zone boundary and various crystal structures, including the heterostructures, the developments of the *ab initio* TPA calculations coupled with the full-band calculations are indispensable.

To our knowledge, there are very few calculations of nonlinear optical properties in materials using the full-band structures. Moss, Sipe, van Driel, and Ghahramani[10–12] calculated both the second- and third-harmonic-generation (SHG and THG) spectra for a number of cubic semiconductors and superlattices, using the empirical tight-binding model and the *semi-ab-initio* linear-combination-of-atomic-orbitals method. Levine and Allan[13,14] have calculated the zero-frequency-limit SHG magnitude of Si, Ge, AlP, AlAs, GaP, and GaAs, using the *ab initio* pseudopotential method in the local-density approximation (LDA) with a self-energy correction in the form of a scissors operator including local-field effects. Huang and Ching[15] have calculated the SHG and THG spectra of various cubic semiconductors, using the orthogonalized linear-combination-of-atomic-orbitals method in the LDA with a scissors operator but without the corresponding self-energy correction. With respect to the TPA, Vaidyanathan, Guenther, and Mitra[16] were the only ones who used the empirical pseudopotential method but obtained TPA coefficients much larger than the measured data for GaAs, InP, CdTe, and ZnSe at particular photon energies.

In the previous communication,[17] we have demonstrated the usefulness of the *ab initio* TPA calculation by computing the degenerate (e.g., single-beam) TPA spectra of Si, ZnSe, and GaAs in a wide photon-energy range. In this calculation, however, two nonlocal corrections to the local momentum operator, which originate from the nonlocalities of the *ab initio* pseudopotentials[18] and self-energy,[13] have not been incorporated into the evaluation of momentum-matrix elements. The purpose of the present paper is to present in detail the method of the *ab initio* TPA calculation, which fully includes the above-mentioned nonlocal corrections, and to compare calculated results with available experiments, including a variety of TPA properties such as the nondegenerate (two-beam) TPA spectra and anisotropy. Our *ab initio* TPA calculation is performed by first computing the band structures of semiconductors by means of the *ab initio* pseudopotential method in the LDA, followed by the numerical evaluation of the third-order nonlinear suscep-

0163-1829/95/52(7)/4986(12)/$06.00

tibility, $\chi^{(3)}$, based on the microscopic response theory.

The rest of the paper is organized as follows. In Sec. II, after giving the expression of the TPA coefficient, we describe numerical details of the TPA spectra calculation, especially the evaluation of momentum-matrix elements in $\chi^{(3)}$. The exact formula of $\chi^{(3)}$ is given in the Appendix. In Sec. III the calculated results with respect to the degenerate and nondegenerate TPA spectra and the anisotropy of various semiconductors are presented and compared with previous experiments and theoretical works. Section IV is devoted to a brief summary.

II. METHOD OF CALCULATIONS

A. Two-photon absorption coefficients

Nonlinear optical processes can often be described in terms of the nonlinear susceptibilities, $\chi^{(n)}$, which are the response functions of the induced polarization with respect to the products of applied electric fields. In the TPA process in cubic-symmetry materials, one has to know the third-order polarization, $P_a^{(3)}(\mathbf{q}_1,\omega_1)$, which is written by

$$P_a^{(3)}(\mathbf{q}_1,\omega_1) = 3\chi^{(3)}_{aaaa}(\mathbf{q}_1,\omega_1;-\mathbf{q}_1,-\omega_1,\mathbf{q}_1,\omega_1,\mathbf{q}_1,\omega_1)|E_a(\mathbf{q}_1,\omega_1)|^2E_a(\mathbf{q}_1,\omega_1) + 6\chi^{(3)}_{abba}(\mathbf{q}_1,\omega_1;-\mathbf{q}_2,-\omega_2,\mathbf{q}_2,\omega_2,\mathbf{q}_1,\omega_1)|E_b(\mathbf{q}_2,\omega_2)|^2E_a(\mathbf{q}_1,\omega_1)(1-\delta_{ab}\delta_{\mathbf{q}_1\mathbf{q}_2}\delta_{\omega_1\omega_2}). \quad (2.1)$$

Here $E_a(\mathbf{q}_1,\omega_1)$ and $E_b(\mathbf{q}_2,\omega_2)$ are complex amplitudes of the probe- and pump-light fields having wave vectors and frequencies, $(\mathbf{q}_1,\omega_1)$ and $(\mathbf{q}_2,\omega_2)$, respectively. Polarization directions, a and b, denote the crystallographic axes, x, y, and z. The numerical prefactors are the degeneracy factors determined by the number of distinct permutations of the applied fields.[1,2] From now on, the long-wavelength approximation ($\mathbf{q}=0$) is adopted because the light considered in this work has a wavelength large compared to the crystal unit cell, and the $\mathbf{q}$ variables are omitted in the following expressions.

The TPA coefficient, β, is a linearly dependent part of the total absorption coefficient, α, on the light intensities, $I_a(\omega_1)$ and $I_b(\omega_2)$, and defined by

$$\alpha^{(3)}(\omega_1) = \beta_{aa}(\omega_1;\omega_1)I_a(\omega_1) + 2\beta_{ab}(\omega_1;\omega_2)I_b(\omega_2)(1-\delta_{ab}\delta_{\omega_1\omega_2}), \quad (2.2)$$

where $\alpha^{(3)}(\omega_1)$ is the third-order absorption coefficient. $\beta_{aa}(\omega_1;\omega_1)$ corresponds to the first self-action term in Eq. (2.1) and is called the degenerate TPA coefficient, while $\beta_{ab}(\omega_1;\omega_2)$ corresponds to the second cross-action term in Eq. (2.1) and is called the nondegenerate one. Together with the degeneracy factors in Eq. (2.1), this definition ensures that the degenerate $\beta_{aa}(\omega_1;\omega_1)$ can be obtained continuously from the nondegenerate $\beta_{aa}(\omega_1;\omega_2)$ as ω_2 approaches ω_1. In the absence of linear absorption where the probe-light energy is below the band-gap energy ($\hbar\omega_1 \le E_g$), we express β exactly as

$$\beta_{ab}(\omega_1;\omega_2) = \frac{6(2\pi)^2\omega_1}{\eta_{aa}(\omega_1)\eta_{bb}(\omega_2)c^2}\mathrm{Im}\chi^{(3)}_{abba}(\omega_1;-\omega_2,\omega_2,\omega_1), \quad (2.3)$$

where $\eta_{aa}(\omega_1)$ and $\eta_{bb}(\omega_2)$ are the frequency-dependent linear refractive indices, c the light velocity, and we have used familiar relations, $I_a(\omega_1) = c\eta_{aa}(\omega_1)|E_a(\omega_1)|^2/2\pi$, etc.

The general formula of $\mathrm{Im}\chi^{(3)}$ is derived from the microscopic response theory and given in the Appendix. Especially in the TPA case, neglecting the local-field effect and adopting the one-particle approximation,

$$\mathrm{Im}\chi^{(3)}_{abba}(\omega_1;-\omega_2,\omega_2,\omega_1) = \frac{1}{6}\left(\frac{1}{\hbar}\right)^3\left(\frac{e}{m_0}\right)^4\frac{\pi}{\omega_1^2\omega_2^2}\int\frac{d\mathbf{k}}{(2\pi)^3}\sum_c\sum_v \times\left|\sum_m\left(\frac{P^a_{vm}(\mathbf{k})P^b_{mc}(\mathbf{k})}{\omega_{mv}(\mathbf{k})-\omega_1}+\frac{P^b_{vm}(\mathbf{k})P^a_{mc}(\mathbf{k})}{\omega_{mv}(\mathbf{k})-\omega_2}\right)\right|^2\delta[\omega_{cv}(\mathbf{k})-\omega_1-\omega_2]. \quad (2.4)$$

Here $e(m_0)$ is the electron charge (mass), v, c, and m are band indices for the valence, conduction, and intermediate states, respectively. $P^a_{vm}(\mathbf{k})$ is the a-component matrix element of the momentum operator, $P^a_{vm}(\mathbf{k}) = \langle v\mathbf{k}|\hat{p}^a|m\mathbf{k}\rangle$, $\omega_{mv}(\mathbf{k})$ is the energy difference between two Bloch states, $|m\mathbf{k}\rangle$ and $|v\mathbf{k}\rangle$.

Many-body effects beyond one-particle approximation, such as local-field effect and excitonic effect, are sometimes important for optical excitations in semiconductors. However, studies of these effects on the nonlinear optical properties in semiconductors are few at the present stage. Levine and Allan[13,14] showed by the *ab initio* calculation that the local-field effect decreases the static SHG magnitude of semiconductors by about 10%, as well as their static dielectric constants. On the other hand, the model-band studies by Weiler[19] and Lee and

Fan[20] showed that the excitonic effect enhances the TPA magnitude by a factor of 2 near the absorption edge. All these effects are not included in the present calculation.

B. Numerical details

To evaluate the momentum-matrix elements and energy denominators in $\mathrm{Im}\chi^{(3)}$, we carried out the self-consistent pseudopotential band-structure calculation within the LDA,[21,22] using the *ab initio* pseudopotentials constructed by Bachelet, Hamann, and Schlüter.[23] For the exchange-correlation potential, we adopted the density-functional form of Ceperly and Alder[24] as parametrized by Perdew and Zunger.[25] The spin-orbit interaction is not included. The momentum-space formalism[26] is employed, where the wave functions are expanded in plane waves with energy less than 12.96 Ry. The details are described elsewhere.[27] A scissors operator is applied to the conduction-band states to address the problem of the band-gap underestimation associated with the LDA. The shift values are 0.668 eV for Si, 0.430 eV for ZnSe, and 0.823 eV for GaAs, which are evaluated to coincide with the experimental values:[28,29] the indirect band-gap energy, 1.17 eV for Si, and the direct band-gap energies, 2.82 eV for ZnSe and 1.52 eV for GaAs. This correction is justified for the present level of study[15] because accurate quasiparticle calculations show a more or less uniform shift in the conduction bands without a substantial change in their wave functions.[30,31]

On calculating $\mathrm{Im}\chi^{(3)}$, two kinds of numerical convergence must be checked carefully. The first one is related to the number of intermediate bands taken in Eq. (2.4). As for the sum of the valence bands, all calculated ones in the pseudopotential scheme are included. This is practically because we use pseudopotentials and physically because the effect of core states on the polarization is small.[30] Therefore we have only to check the convergence of $\mathrm{Im}\chi^{(3)}$ as a function of the number of intermediate conduction bands included. The result is given in Table I for ZnSe at two particular photon energies. It is seen that more conduction bands should be taken into the calculation when we consider the higher-energy light; the higher-energy transition. We found that 26 conduction bands are appropriate for zinc-blende semiconductors studied in this work. The residual errors due to this truncation are estimated about 1%.

TABLE I. Convergence of $\mathrm{Im}\chi^{(3)}_{xxxx}(\omega;-\omega,\omega,\omega)$ as a function of the number of conduction bands included. Data are for the case of ZnSe at $\hbar\omega = 1.8$ and 2.6 eV using $36\times36\times36$ **k** points in the fcc Brillouin zone. Unit is 10^{-12} esu.

Number of bands	1.8 (eV)	2.6 (eV)
1	3.3324	4.8493
4	3.2612	6.4866
8	3.7881	7.0925
20	3.8363	7.2119
26	3.8526	7.2367
38	3.8521	7.2486

TABLE II. Convergence of $\mathrm{Im}\chi^{(3)}_{xxxx}(\omega;-\omega,\omega,\omega)$ as a function of the number of **k** points in the fcc Brillouin zone. Data are for the case of ZnSe at $\hbar\omega = 1.8$ and 2.6 eV using 26 conduction bands. Unit is 10^{-12} esu.

Number of **k** points	1.8 (eV)	2.6 (eV)
$24\times24\times24$	3.7621	7.0949
$36\times36\times36$	3.8526	7.2367
$48\times48\times48$	3.8703	7.2686

The second convergence is related to the sum over the Brillouin zone in Eq. (2.4). In this work the tetrahedron method[32] is adopted and a whole fcc Brillouin zone is divided with $n\times n\times n$ mesh **k** points. Table II gives the convergence of $\mathrm{Im}\chi^{(3)}$ as a function of the number of these **k** points. This table shows that $48\times48\times48$ mesh **k** points are appropriate, which corresponds to 2769 points in the irreducible Brillouin zone and 663 552 tetrahedra in a whole Brillouin zone. This truncation is estimated to have 3–5 % errors in the calculated $\mathrm{Im}\chi^{(3)}$.

To calculate the TPA coefficient, the linear refractive index $\eta_{aa}(\omega)$ also needs to be evaluated. For this purpose, we first calculate the imaginary part of the dielectric function, $\varepsilon_{2,aa}(\omega)$, in a similar manner to $\mathrm{Im}\chi^{(3)}$. Then its real part, $\varepsilon_{1,aa}(\omega)$, is obtained from $\varepsilon_{2,aa}(\omega)$ by the Kramers-Krönig transformation.[33] In this way, $\eta_{aa}(\omega)$ is given by $[\varepsilon_{1,aa}(\omega)]^{1/2}$ when $\hbar\omega$ is below the band-gap energy.

C. Momentum-matrix element

In the calculation of momentum-matrix elements, $P^a_{mn}(\mathbf{k})$, two nonlocal corrections should be added to the local momentum operator, $\hat{p}^a_{\mathrm{loc}} = \hbar/i\cdot\nabla_a$, in order to preserve the gauge invariance of an optical transition rate[34] such as

$$\hat{p}^a = \hat{p}^a_{\mathrm{loc}} + \frac{m}{\hbar}[\hat{V}_{\mathrm{nl}}, i\hat{x}^a] + \frac{m}{\hbar}[\hat{\Sigma}, i\hat{x}^a]. \tag{2.5}$$

Here $\hat{V}_{\mathrm{nl}}$ and $\hat{\Sigma}$ are the nonlocal pseudopotential and the nonlocal self-energy, respectively, and $\hat{x}^a$ is the a component of the position operator.

The pseudopotential correction is intrinsic to the nonlocal pseudopotential scheme. Systematic analysis of this correction was performed by Read and Needs[18] for the optical momentum-matrix elements between the orbitals of various isolated atoms. For the optical properties of bulks, its relevance was demonstrated in the calculation of the static dielectric constant $\varepsilon_1(0)$.[35] To calculate this correction the analytic form in the momentum space derived by Hybertsen and Louie[35] is employed, where the matrix element between the plane waves, $|\mathbf{q}\rangle$ and $|\mathbf{q}'\rangle$, is given by

$$\langle\mathbf{q}|\frac{m}{\hbar}[\hat{V}_{\mathrm{nl}}, i\hat{x}^a]|\mathbf{q}'\rangle = \frac{m}{\hbar}\left(\frac{\partial}{\partial \mathrm{q}^a} + \frac{\partial}{\partial \mathrm{q}'^a}\right)\langle\mathbf{q}|\hat{V}_{\mathrm{nl}}|\mathbf{q}'\rangle. \tag{2.6}$$

On the other hand, the self-energy correction is intrinsic to the calculation of optical momentum-matrix elements using one-particle wave functions, which is called the velocity renormalization based on the Ward-Takahashi identity. Levine and Allan[13] pointed out its significance in the realistic calculation, proposed the simple recipe to evaluate this correction, which is useful in the case of using the scissors operator as the addition of self-energy, and demonstrated its relevance in the calculations of the lower-energy $\varepsilon_1(\omega)$ and $\chi^{(2)}(0)$.[13,14] In the present work, we follow their approach using the factorized-replacement form for the momentum-matrix element between the valence- and conduction-band states such as

$$P^a_{vc}(\mathbf{k}) = \left(1 + \frac{\Delta}{\omega_c^{\mathrm{LDA}}(\mathbf{k}) - \omega_v^{\mathrm{LDA}}(\mathbf{k})}\right) \times \langle v\mathbf{k}|\hat{p}^a_{\mathrm{loc}} + \frac{m}{\hbar}[\hat{V}_{\mathrm{nl}}, i\hat{x}^a]|c\mathbf{k}\rangle, \quad (2.7)$$

where $\omega_c^{\mathrm{LDA}}(\mathbf{k})$ is the LDA energy of the state $|c\mathbf{k}\rangle$ and Δ is the scissors-shift energy.

First we display the numerical importance of these two nonlocal corrections in the present optical-transition-rate calculations. Figures 1(a)–1(c), respectively, show the calculated $\mathrm{Im}\chi^{(3)}_{xxxx}(\omega;-\omega,\omega,\omega)$, $\varepsilon_{1,xx}(\omega)$, and $\varepsilon_{2,xx}(\omega)$ for ZnSe in the TPA photon-energy region, where the values with and without corrections are displayed. It is clearly seen that both the pseudopotential and self-energy corrections change the transition rates in $\mathrm{Im}\chi^{(3)}$, ε_1, and ε_2 by definite ratios (5–30 %).

To clarify the material and transition-energy dependence of these corrections, the calculated (partially corrected $\mathrm{Im}\chi^{(3)}$)/(fully corrected $\mathrm{Im}\chi^{(3)}$) ratios are shown in Fig. 2 for GaAs, ZnSe, and Si, as functions of photon energy.

First, we note that the pseudopotential correction strongly depends on the materials; the correction value is negative and large (20–30 %) for Si, while positive and small (5–10 %) for ZnSe and GaAs. This feature is also seen in the calculated momentum-matrix elements between s- and p-pseudo-orbitals of isolated atoms. Second, the effect of the pseudopotential correction is nearly independent of the transition energy, thus the individual types of transitions (E_0, E_1, etc.) in the Bril-

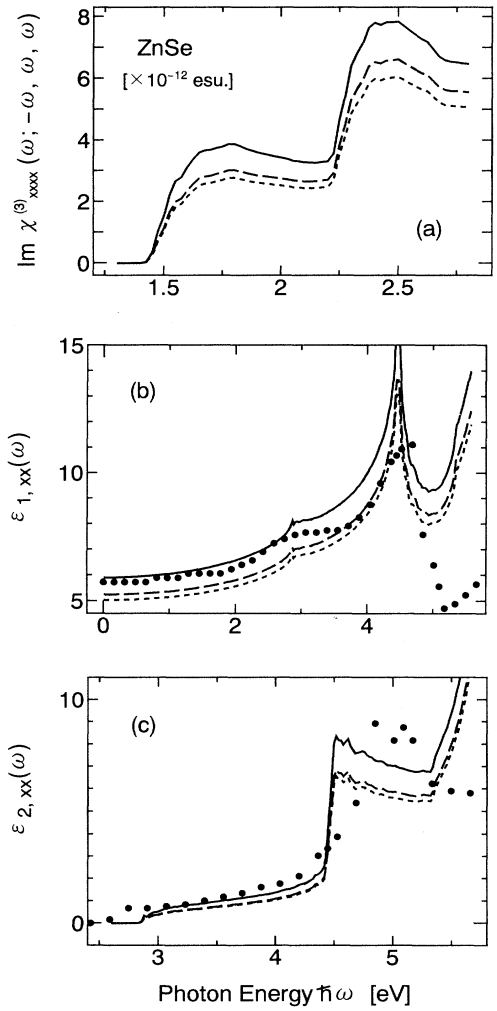

FIG. 1. Effects of the nonlocal pseudopotential and self-energy corrections on (a) $\mathrm{Im}\chi^{(3)}_{xxxx}(\omega;-\omega,\omega,\omega)$, (b) $\varepsilon_{1,xx}(\omega)$, and (c) $\varepsilon_{2,xx}(\omega)$ for ZnSe. Dotted lines are evaluated by using only matrix elements of local momentum operator, dashed lines with nonlocal pseudopotential correction, and solid lines with full (pseudopotential + self-energy) corrections. Filled circles are experimental data from Ref. 36.

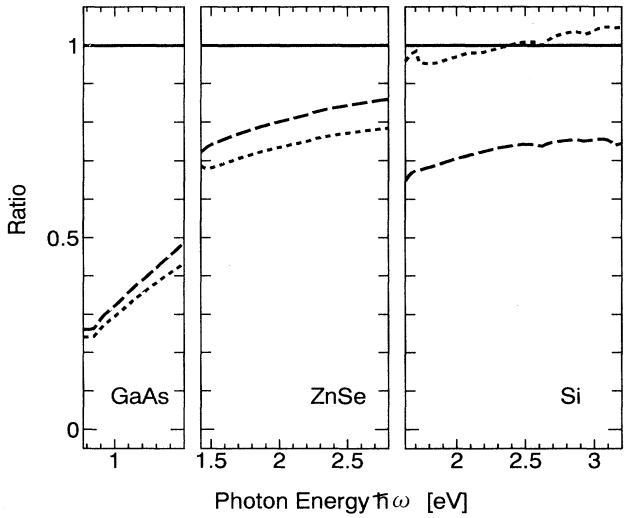

FIG. 2. Material dependence of the effects of nonlocal pseudopotential and self-energy corrections on $\mathrm{Im}\chi^{(3)}_{xxxx}(\omega;-\omega,\omega,\omega)$ for Si, ZnSe, and GaAs as a function of photon energy. Dotted lines, $\mathrm{Im}\chi^{(3)}$ with only the local momentum operator; dashed lines, $\mathrm{Im}\chi^{(3)}$ with the nonlocal pseudopotential correction; and solid lines as a unit, fully-corrected $\mathrm{Im}\chi^{(3)}$ with the nonlocal pseudopotential and self-energy corrections.

TABLE III. Static dielectric constants $\varepsilon_{1,xx}(0)$ calculated with and without the nonlocal corrections on the momentum operator. The results in the upper three rows are obtained as the static limit of $\varepsilon_{1,xx}(\omega)$ transformed from $\varepsilon_{2,xx}(\omega)$. The results described as direct calculation and by Levine and Allan are evaluated directly by using the real-part formula of $\varepsilon_{1,xx}(0)$. Experimental results are also presented.

	Si	ZnSe	GaAs
only $\hat{p}^a_{\rm loc}$	10.18	5.02	6.96
with $m[\hat{V}_{\rm nl}, i\hat{x}^a]/\hbar$	8.79	5.24	7.49
with $m[\hat{V}_{\rm nl}+\hat{\Sigma}, i\hat{x}^a]/\hbar$	11.64	5.90	10.77
direct calculation	11.73	5.90	10.88
Levine and Allan			
without local field	11.8[a]		11.54[b]
with local field	11.3[a]		11.00[b]
experiment	12.1,[c] 11.7[c]	5.6[d]	10.9[c]

[a]Reference 13.
[b]Reference 14.
[c]Reference 28.
[d]Reference 29.

louin zone. This may be explained by considering that most such transitions have the single character of transitions from the bonding-p-like upper-valence bands to the antibonding-s-like lower-conduction ones.

On the other hand, the self-energy correction increases the transition rate in $\mathrm{Im}\chi^{(3)}$ for all semiconductors. This is because in the present treatment of self-energy the positive energy shift of conduction bands always increases the momentum-matrix elements between valence- and conduction-band states by the factor $\Delta/[\omega_c^{\rm LDA}(\mathbf{k})-\omega_v^{\rm LDA}(\mathbf{k})]$. With respect to the absorption-edge transitions in various semiconductors, such factors are 0.668 eV/2.578 eV $\sim$ 0.26, 0.430 eV/2.390 eV $\sim$ 0.18, and 0.823 eV/0.697 eV $\sim$ 1.18 for Si, ZnSe, and GaAs, respectively. Thus the self-energy correction is largest for GaAs. Moreover, the self-energy correction strongly depends on the transition energy such that it decreases the transition rate with increasing the transition energy.

Finally, the test of our calculation is presented by comparing the calculated linear optical properties with previous calculation. Table III shows the calculated and observed static dielectric constants, $\varepsilon_{1,xx}(0)$. The above-mentioned features of two nonlocal corrections are also seen in the present results in this table. Considering that different values are used as scissors-shift energies between the present and previous calculations, the present results with full corrections are in good agreement with early ones.[13,14]

III. NUMERICAL RESULTS

A. Degenerate TPA

With respect to degenerate TPA spectra, the calculated results and detailed discussion have already been reported.[17] Thus, here, we confine our attention to the comparison of the present improved results using two nonlocal corrections with previous results without corrections and experiments. Figures 3(a), 3(b), and 3(c), respectively, show the calculated degenerate TPA coefficients, $\beta_{xx}(\omega;\omega)$, for Si, ZnSe, and GaAs as a function of the probe-light energy. In these figures, down arrows indicate the calculated interband energies corresponding to the *onsets* of E_0, E_0', E_1, E_1', and E_2 transitions, which are summarized in Table IV. As seen in these figures, for ZnSe and GaAs, the TPA magnitude is greatly increased

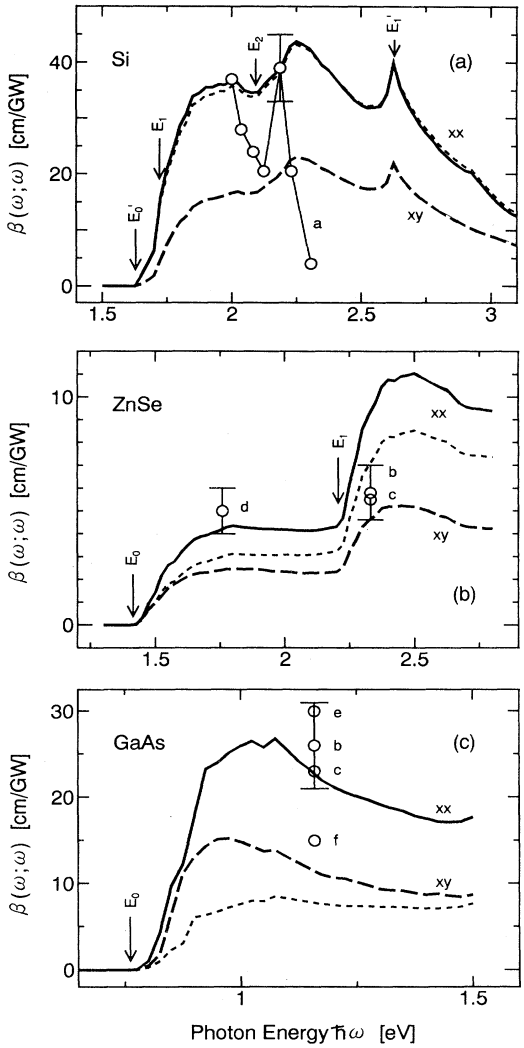

FIG. 3. Calculated degenerate TPA coefficients, $\beta(\omega;\omega)$, of Si (a), ZnSe (b), and GaAs (c) as a function of photon energy. Solid and dotted lines are, respectively, $\beta_{xx}(\omega;\omega)$ with and without nonlocal corrections, the latter of which corresponds to the previous publication. (Ref. 37) Experimental data (open circles), a, b, c, d, e, and f, are from Refs. 38, 39, 40, 41, 42, and 43, respectively. Dashed lines show the different polarizations, $\beta_{xy}(\omega;\omega)$.

TABLE IV. Calculated interband energies (eV) in various critical-point transitions observed in TPA.

	Si	ZnSe	GaAs
E_0 $(\Gamma_{1c}-\Gamma_{15v})$		2.820	1.520
E_0' $(\Gamma_{15c}-\Gamma_{15v})$	3.246		
E_1 $(L_{1c}-L_{3v})$	3.431	4.413	
E_1' $(L_{3c}-L_{3v})$	5.247		
E_2 $(X_{13c}-X_{5v})$	4.186		

by the nonlocal corrections and the improved results are in excellent agreement with reliable experimental data.

Although two nonlocal corrections significantly increase the TPA magnitude, our previous analysis of the spectral shape and peak position in $\beta_{xx}(\omega;\omega)$ and $\varepsilon_{2,xx}(\omega)$ is available for the present results. According to Ref. 17, their scaling-functional forms on the photon energy $\hbar\omega$ are written for the M_m transition above its critical-point energy, E_m^c, as follows:

$$\beta_{xx}^m(\omega;\omega) \sim \pm\frac{(2\hbar\omega/E_m^c-1)^{|1-m|/2+x}}{(2\hbar\omega/E_m^c)^5}, \tag{3.1}$$

$$\varepsilon_{2,xx}^m(\omega) \sim \pm\frac{(\hbar\omega/E_m^c-1)^{|1-m|/2}}{(\hbar\omega/E_m^c)^2}, \tag{3.2}$$

where $m = 0$ and 1 correspond to a positive sign, while $m = 2$ corresponds to a negative one, and x represents the degree of forbidden transition. Figures 4(a)–4(c), respectively, illustrate these forms for $m = 0$, 1, and 2. From these figures, it is easily recognized that the E_0 peak in $\beta_{xx}(\omega;\omega)$ appears at lower energy $[2\hbar\omega = 10/(9-2x)E_0^c]$ than that in $\varepsilon_{2,xx}(\omega)$ $(\hbar\omega = 4/3E_0^c)$ and the steplike E_1 peak in $\varepsilon_{2,xx}(\omega)$ at $\hbar\omega = E_1^c$ shifts to higher energy $[2\hbar\omega = 5/(5-x)E_1^c]$ and broadens in $\beta_{xx}(\omega;\omega)$, while the E_2 peaks in $\varepsilon_{2,xx}(\omega)$ and $\beta_{xx}(\omega;\omega)$ have the same position at E_2^c. These results clearly explain the calculated spectral features in Si, ZnSe, and GaAs. [With respect to $\varepsilon_{2,xx}(\omega)$, see the figures in Ref. 17.]

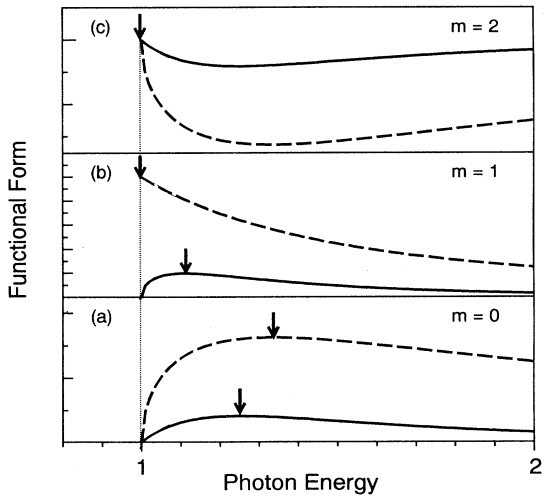

FIG. 4. Scaling-functional forms of $\beta_{xx}^m(\omega;\omega)$ (solid lines) and $\varepsilon_{2,xx}^m(\omega)$ (dashed lines) for transition types, $m = 0, 1$, and 2. $\beta_{xx}^m(\omega;\omega)$ is shown as a function of $2\hbar\omega/E_m^c$, while $\varepsilon_{2,xx}^m(\omega)$ is shown as a function of $\hbar\omega/E_m^c$. Down arrows indicate the peak positions. The value x in Eqs. (3.1) and (3.2) is taken to be 0.5.

B. Nondegenerate TPA

Off-diagonal tensor elements such as $\beta_{xy}(\omega;\omega)$ are classfied as nondegenerate TPA coefficients. In Figs. 3(a), 3(b), and 3(c), we have shown the calculated $\beta_{xy}(\omega;\omega)$ as a function of photon energy for Si, ZnSe, and GaAs, respectively. As seen in these figures, $\beta_{xy}(\omega;\omega)$ is always smaller than $\beta_{xx}(\omega;\omega)$ but has no remarkable spectral characteristics compared with $\beta_{xx}(\omega;\omega)$. The former feature will be discussed in detail when we consider the anisotropy in the next section.

$\beta_{xx}(\omega_1;\omega_2)$ and $\beta_{xy}(\omega_1;\omega_2)$ belong to another type of nondegenerate TPA coefficient having different probe- and pump-light energies. Figure 5 shows the calculated nondegenerate $\beta(\omega_1;\omega_2)$ for ZnSe as a function of the probe-light energy, $\hbar\omega_1$, where the pump-light energy is fixed at $\hbar\omega_2 = 1.759$ eV. Down arrows indicate the absorption onsets, E_0 and E_1, which are 1.061 and 2.654 eV, respectively. As compared with the degenerate TPA results for the same material in Fig. 3(b), the E_0 and E_1 absorption edges move to lower and higher energies, respectively, and the spectrum has no apparent peak in the E_0-transition region below the E_1 edge. These are because the resonance in $\beta(\omega_1;\omega_2)$ occurs at the sum frequency, $\omega_1+\omega_2$, in the nondegenerate TPA case, and $\beta(\omega_1;\omega_2)$ has the different ω_1 dependence from that of the degenerate $\beta(\omega_1;\omega_1)$. Comparing with the previous

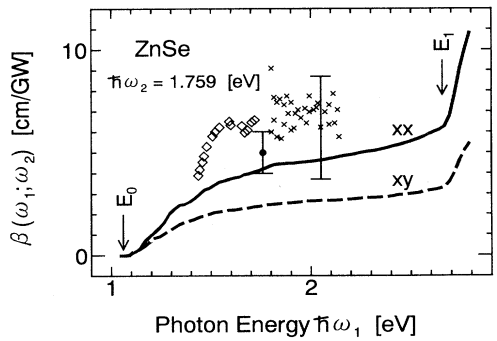

FIG. 5. Calculated nondegenerate $\beta(\omega_1;\omega_2)$ of ZnSe as a function of probe-light energy $\hbar\omega_1$. Pump-light energy $\hbar\omega_2$ is fixed at 1.759 eV. Solid and dashed lines show the different polarizations, $\beta_{xx}(\omega_1;\omega_2)$ and $\beta_{xy}(\omega_1;\omega_2)$, respectively. Open diamonds and crosses are experimental data with different pump-light intensities, while the filled circle is the result of an independent degenerate TPA experiment. These data are from Ref. 41.

measurements[41] shown in Fig. 5, the calculated results look slightly small but are within the experimental accuracy.

The nondegenerate $\beta_{xx}(\omega_1;\omega_2)$ spectra of ZnS were also measured for a zinc-blende sample,[41] which are shown in the inset of Fig. 6. However, in this experiment, the possibility of the sample being polycrystals made of zinc-blende and wurtzite structures was suggested. The present *ab initio* approach applies to materials having any crystal structures. Therefore, in order to clarify the TPA-spectra difference between zinc-blende and wurtzite structures, we have evaluated $\beta_{xx}(\omega_1;\omega_2)$ in the zinc-blende structure and $\beta_{xx}(\omega_1;\omega_2)$ and $\beta_{zz}(\omega_1;\omega_2)$ in the wurtzite structure.[44] Note that $\beta_{zz}(\omega_1;\omega_2)$ is equal to $\beta_{xx}(\omega_1;\omega_2)$ in the zinc-blende structure. The results are shown in Fig. 6, where down arrows indicate E_0 (1.924 eV) and E_1 (3.369 eV) onset energies in the zinc-blende structure. The calculated band-gap energy in the wurtzite structure, $\Gamma_{1c}-\Gamma_{6v}$, is slightly larger than that in the zinc-blende one, $\Gamma_{1c}-\Gamma_{15v}$, by 0.025 eV.

As seen in the inset of Fig. 6, the calculated spectra $\beta_{xx}(\omega_1;\omega_2)$ in zinc-blende and wurtzite structures have comparable magnitude around the absorption edges. This is because the electronic-structure difference between both crystal structures is small for semiconductors having large ionicity such as ZnS.[27] As a result, these spectra are within the experimental accuracy, and thus it is difficult to judge the degree of polycrystallization in an experimental sample by comparing the calculated results with experimental ones. However, the definite difference of magnitude is recognized between the calculated $\beta_{xx}(\omega_1;\omega_2)$ and $\beta_{zz}(\omega_1;\omega_2)$ in a higher-energy region for wurtzite ZnS. Then, as one way to clarify the polycrystallization, we propose the measurements of both $\beta_{xx}(\omega_1;\omega_2)$ and $\beta_{zz}(\omega_1;\omega_2)$ in a higher-energy region.

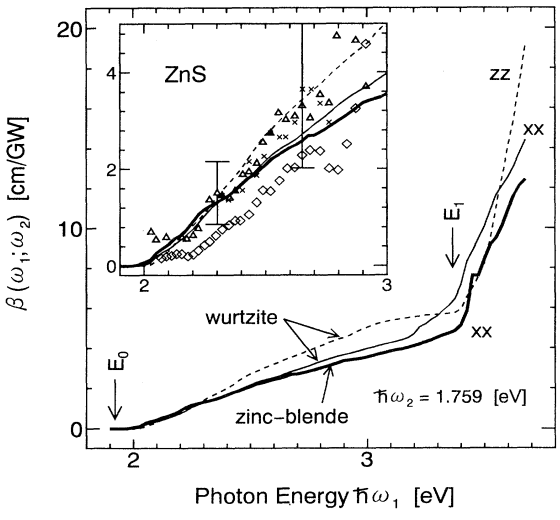

FIG. 6. Calculated nondegenerate $\beta(\omega_1;\omega_2)$ of zinc-blende and wurtzite ZnS as a function of probe-light energy $\hbar\omega_1$. Pump-light energy $\hbar\omega_2$ is fixed at 1.759 eV. Solid and dashed lines show the different polarizations, $\beta_{xx}(\omega_1;\omega_2)$ and $\beta_{xy}(\omega_1;\omega_2)$, respectively. Open diamonds, open triangles, and crosses are experimental data with different pump-light intensities from Ref. 41.

C. Anisotropy

For materials having cubic symmetry such as T_d ($\bar{4}3m$), $\chi^{(3)}$ has four independent nonzero tensor elements, $\chi^{(3)}_{xxxx}$, $\chi^{(3)}_{xyyx}$, $\chi^{(3)}_{xyxy}$, and $\chi^{(3)}_{xxyy}$.[1,2] Especially in the *frequency*-degenerate TPA described by $\chi^{(3)}(\omega;-\omega,\omega,\omega)$, $\chi^{(3)}_{xyxy}$ is equal to $\chi^{(3)}_{xyyx}$, thus there exist only three independent elements. In this subsection, we consider the anisotropy in such frequency-degenerate TPA.

First we consider the calculated ratios:

$$A \equiv \frac{\mathrm{Im}\chi^{(3)}_{xyyx}}{\mathrm{Im}\chi^{(3)}_{xxxx}}, \qquad B \equiv \frac{\mathrm{Im}\chi^{(3)}_{xxyy}}{\mathrm{Im}\chi^{(3)}_{xxxx}}, \tag{3.3}$$

which are shown for GaAs, ZnSe, and Si in Fig. 7. The following common features are found among these semiconductors. (1) In the E_0-transition regions of GaAs and ZnSe, with increasing the photon energy, the ratio A decreases sharply in the lower-energy side and gradually in the higher-energy side. On the other hand, the ratio B displays the opposite change, thus increasing sharply and gradually in the lower- and higher-energy sides, respectively. (2) In the E_1-transition regions of ZnSe and Si, B decreases with increasing the photon energy while the variation of A is small. (3) In the lower-energy sides of the E_0'- and E_2-transition regions of Si, both A and B

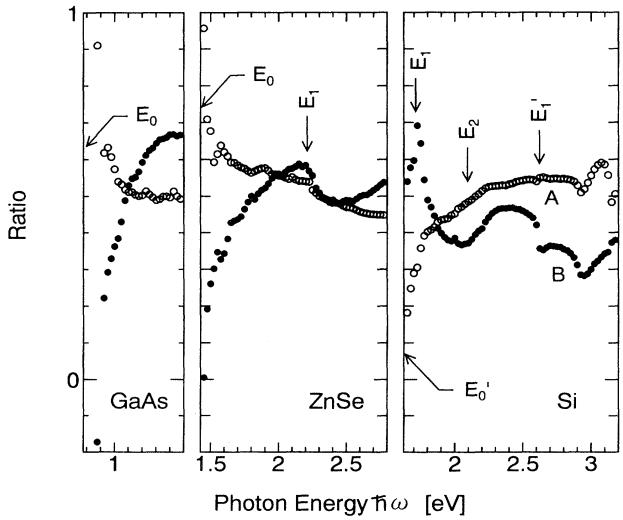

FIG. 7. Ratios, $A = \mathrm{Im}\chi^{(3)}_{xyyx}/\mathrm{Im}\chi^{(3)}_{xxxx}$ (open circles) and $B = \mathrm{Im}\chi^{(3)}_{xxyy}/\mathrm{Im}\chi^{(3)}_{xxxx}$ (filled circles), in the frequency-degenerate TPA for GaAs, ZnSe, and Si as a function of photon energy.

increase with increasing the photon energy.

Some of these features are qualitatively explained by considering the symmetry of the respective two-photon transition. For example, only the transition, $\Gamma_{15v} \rightarrow \Gamma_{15c} \rightarrow \Gamma_{1c}$, caused by two photons with different polarizations, such as x and y, is allowed at the center of the Brillouin zone.[45] Thus we expect $\chi^{(3)}_{xyyx} \neq 0$ but $\chi^{(3)}_{xxxx} \sim 0$ at the E_0 absorption edge, which explains why the ratio A has large values at the E_0 absorption edge. On the other hand, because the transition $L_{3v} \rightarrow L_{3c} \rightarrow L_{1c}$ is allowed for two photons with arbitrary polarizations, $\chi^{(3)}_{xxxx}$ as well as $\chi^{(3)}_{xyyx}$ has nonvanishing values at the E_1 absorption edge. This explains that the ratio A does not have such large values at the E_1 edge as those at the E_0 edge.

An experimental setup generally posesses the electromagnetic fields with arbitrary propagation and polarization directions. Therefore, from a practical viewpoint, it is useful to define two independent parameters that describe the TPA anisotropy as follows:[9]

$$\sigma = \frac{\mathrm{Im}\chi^{(3)}_{xxxx} - 2\,\mathrm{Im}\chi^{(3)}_{xyyx} - \mathrm{Im}\chi^{(3)}_{xxyy}}{\mathrm{Im}\chi^{(3)}_{xxxx}}, \tag{3.4}$$

$$\delta = \frac{\mathrm{Im}\chi^{(3)}_{xxxx} - 2\,\mathrm{Im}\chi^{(3)}_{xyyx} + \mathrm{Im}\chi^{(3)}_{xxyy}}{2\,\mathrm{Im}\chi^{(3)}_{xxxx}}. \tag{3.5}$$

Here σ is called the anisotropy parameter while δ is the dichroism parameter. In experiments, σ corresponds to the coefficient of the propagation-polarization-angle-dependent part of the TPA magnitude, while δ is relating to the difference of absorption magnitude between the linearly and circularly polarized lights. Especially in isotropic materials, $\delta=\sigma=0$.

The calculated $-\sigma$ and δ are shown in Figs. 8 and 9,

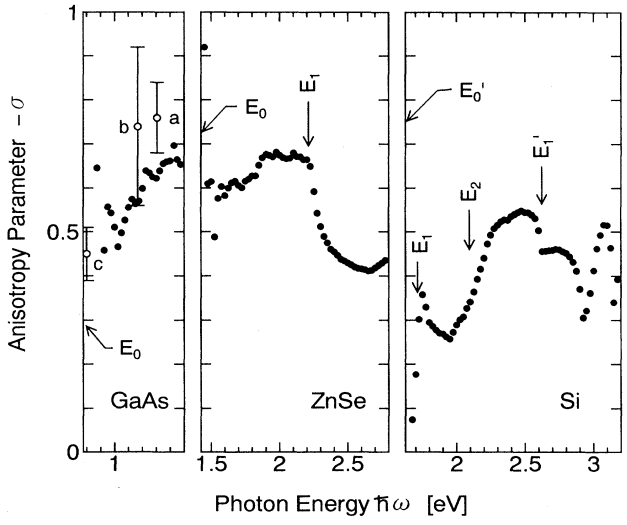

FIG. 8. Calculated TPA anisotropy parameter, $-\sigma$, for GaAs, ZnSe, and Si as a function of photon energy. Filled circles are the present results and open circles are experimental data from Refs. 46 (a), 47 (b), and 45 (c).

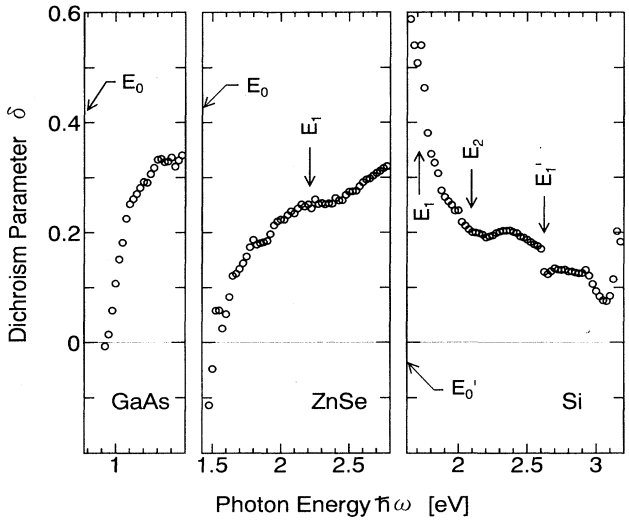

FIG. 9. Calculated TPA dichroism parameter, δ, for GaAs, ZnSe, and Si as a function of photon energy.

respectively, for GaAs, ZnSe, and Si. It is seen that $-\sigma$ gradually increases in the E_0-transition region with increasing the photon energy. This is because the compensation occurs between the variations in the ratios, A and B, while $-\sigma$ decreases/increases sharply in the E_1/E_2-transition region due to the cooperative variations in A and B. With respect to δ, these features, compensation and cooperation, are found to be opposite to $-\sigma$, thus showing sharp change in the E_0-transition region while showing no characteristic change in the E_1- and E_2-transition regions.

The experimental data are available only for $-\sigma$ in GaAs, which are shown in Fig. 8. Compared with these experiments, the calculated results show good agreement in the lower-energy region, while they give slightly small values in the higher-energy region. The reason for this discrepancy is not clear at present.

D. Comparison to previous works

Now we preface the discussion of the comparison of the present calculations to previous works. Although numerous model-band calculations of TPA spectra have been performed, several recent calculations are noteworthy because these calculations were successful in giving the TPA magnitude comparable to recent accurate experiments. Hutching and Van Stryland[8] have presented the TPA-coefficient calculation by using the second-order perturbation theory and a Kane band-structure model consisting of three valence bands and one conduction band. Although this model-band calculation explains well the TPA magnitude of various semiconductors, it gives no anisotropy for the TPA spectra, i.e., $\sigma = 0$, contrary to experimental observations.[45] In order to explain the

TPA anisotropy, Hutchings and Wherrett[9] introduced a Luttinger-Kohn band-structure model consisting of three valence bands and four conduction bands.

First we compare the TPA spectra evaluated by using the above-mentioned band-structure models[8,9] with those by the present *ab initio* approach. Figures 10(a) and 10(b), respectively, show the calculated $\beta_{xx}(\omega;\omega)$ for GaAs and ZnSe, as a function of photon energy. The overall agreement on the spectral shape and magnitude is obtained among these calculations. However, the following differences should be noted. (1) The spectral structures originating from the Brillouin-zone-boundary transitions, such as the E_1-transition peak in a higher-energy region of ZnSe, can be evaluated only by the present approach. (2) The incorporation of more than four conduction bands into the calculation is necessary to obtain the fully convergent TPA magnitude. This statement is easily recognized by recalling the results of band-number-convergence check shown in Sec. II B, or by viewing the magnitude difference between model calculations using one and four conduction bands (lines *b* and *a* in Fig. 10).[9]

Figures 11(a) and 11(b), respectively, show the calculated photon-energy dependence of TPA-anisotropy parameters, $-\sigma$ and δ, in GaAs by the Luttinger-Kohn band-structure model[9] and the present *ab initio* approach. Note that the dip structure in a lower-energy region of δ by the model calculations originates from the valence-band splitoff due to the spin-orbit interaction, which is not included in the present *ab initio* calculation. Comparing the calculated δ and $-\sigma$ by the four-conduction-band model with those by the *ab initio* approach, good agreement is seen in a lower-energy region, while a definite difference exists in a higher-energy region. As one of the reasons for this discrepancy, we point out the limitation of the model-band description; although the band-structure range well described by the Luttinger-Kohn model is not well elucidated, such a range is known to be limited around the band-gap energy.[48]

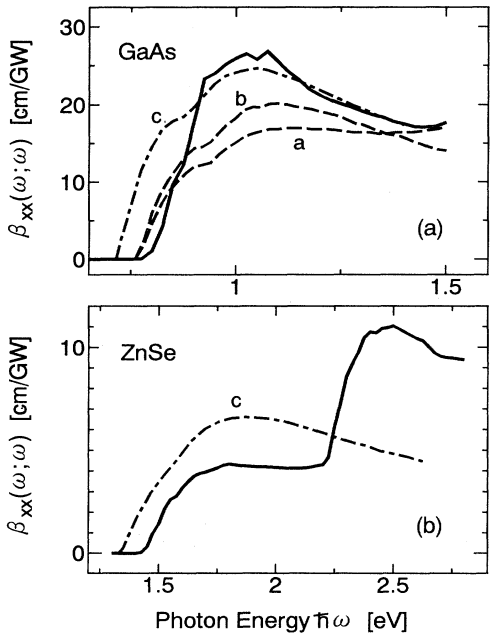

FIG. 10. Comparison to previous calculations for (a) GaAs and (b) ZnSe. Solid lines correspond to the present calculation, dashed lines (*a* and *b*) are evaluated using the Luttinger-Kohn band-structure model in Ref. 9, dot-dashed lines (c) using the Kane band-structure model in Ref. 8. Lines, *a* and *b*, respectively, correspond to the results using four and one lowest conduction bands.

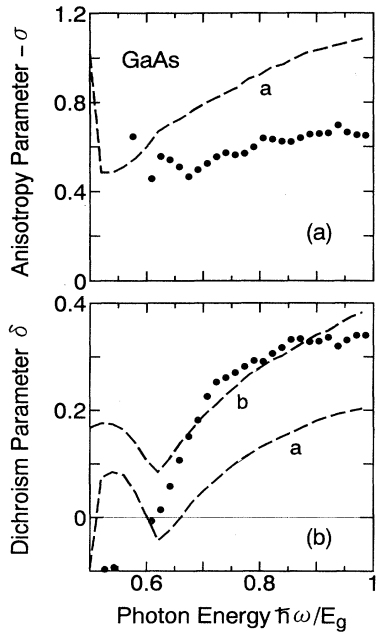

FIG. 11. Comparison to previous calculation for (a) anisotropy and (b) dichroism parameters of GaAs. Filled circles are the present results and dashed lines are evaluated in Ref. 9 using the Luttinger-Kohn band-structure model with four lowest conduction bands (line *a*) and with a single conduction band (line *b*). Anisotropy parameter for the single-conduction-band model is equal to zero [does not appears in (a)].

IV. SUMMARY

Two-photon-absorption (TPA) spectra of various semiconductors have been evaluated by using the *ab initio* full-band structures and the exact microscopic formula of nonlinear susceptibility, $\chi^{(3)}$. We have obtained the following conclusions.

(1) Two nonlocal corrections, the pseudopotential and self-energy corrections, to the momentum-matrix elements are essential for the calculation of $\mathrm{Im}\chi^{(3)}$. The effects of both corrections strongly depend on materials.

(2) The calculated degenerate and nondegenerate TPA spectra for Si, ZnSe, GaAs, and ZnS are in good agree-

ment with the latest experimental data. This fact demonstrates the usefulness and reliability of *ab initio* approach in the TPA-spectra calculation.

(3) Most semiconductors show abundant TPA-spectral structures similar to one-photon absorption (OPA). However, the spectral shape is quite different between TPA and OPA, which can be analyzed using a simple scaling formula for the respective type of critical-point singularity. Moreover, the spectral shape and magnitude are different between degenerate and nondegenerate TPA for the same semiconductor.

(4) The TPA anisotropy is observed in all semiconductors studied here. Its magnitude and photon-energy dependence are found to be quite different among various critical-point transitions. Some of these features can be understood by considering the symmetry of two-photon transitions.

Finally, we expect that availability of the present *ab initio* approach will be important in studying nonlinear optical properties of various materials having complicated crystal structures such as superlattices, surfaces, and microcrystals.

ACKNOWLEDGMENTS

This work was supported by a Grant-in-Aid from the Ministry of Education, Science, and Culture, Japan. One of us (M.M.) gratefully acknowledges support from the Japan Society for the Promotion of Science for Japanese Junior Scientists.

APPENDIX: MICROSCOPIC FORMULA OF $\chi^{(3)}$

In this appendix, we present the microscopic formula of $\chi^{(3)}$ which has the full dependence on the polarizations, wave numbers, and frequencies of applied electromagnetic fields. Using the microscopic response theory or the density-matrix theory, $\chi^{(3)}$ is given by

$$\chi^{(3)}_{abcd}(\mathbf{q}_1,\omega_1;\mathbf{q}_2,\omega_2,\mathbf{q}_3,\omega_3,\mathbf{q}_4,\omega_4)=\frac{1}{|\hat{\mathcal{P}}^{bcd}|}\left(\frac{1}{\hbar}\right)^3\left(\frac{e}{m_0}\right)^4\frac{-1}{\omega_1\omega_2\omega_3\omega_4}\sum_{klmn}e^{-\beta\hbar\omega_n}$$

$$\times\hat{\mathcal{P}}^{abcd}\frac{\langle n|\hat{P}^a(-\mathbf{q}_1)|k\rangle\langle k|\hat{P}^b(\mathbf{q}_2)|l\rangle\langle l|\hat{P}^c(\mathbf{q}_3)|m\rangle\langle m|\hat{P}^d(\mathbf{q}_4)|n\rangle}{(\omega_{kn}-\omega_2-\omega_3-\omega_4)(\omega_{ln}-\omega_3-\omega_4)(\omega_{mn}-\omega_4)},\tag{A1}$$

where $\mathbf{q}_1=\mathbf{q}_2+\mathbf{q}_3+\mathbf{q}_4$ and $\omega_1=\omega_2+\omega_3+\omega_4$. $|k\rangle$'s are many-body electronic states, $\hbar\omega_{kn}\equiv\hbar\omega_k-\hbar\omega_n$ is the energy difference between $|k\rangle$ and $|n\rangle$, and $\beta=1/(k_BT)$ is the inverse thermal energy. The applied (input) electromagnetic fields are characterized by the sets of polarization, wave number, and frequency such as $(b,\mathbf{q}_2,\omega_2)$, $(c,\mathbf{q}_3,\omega_3)$, and $(d,\mathbf{q}_4,\omega_4)$, while the scattered (output) electromagnetic field by $(a,\mathbf{q}_1,\omega_1)$. $\hat{\mathcal{P}}^{abcd}$ is the full permutations operator on the above-mentioned four sets, while $|\hat{\mathcal{P}}^{bcd}|$ is the number of intrinsic permutations of the input three sets. $\hat{P}^a(-\mathbf{q}_1)$ is defined as

$$\hat{P}^a(-\mathbf{q}_1)\equiv\int d\mathbf{x}_1\hat{\psi}^\dagger(\mathbf{x}_1)e^{-i\mathbf{q}_1\mathbf{x}_1}\hat{p}^a\hat{\psi}(\mathbf{x}_1),\tag{A2}$$

where $\hat{p}^a=\hbar/i\cdot\nabla_a$ and $\hat{\psi}(\mathbf{x}_1)$ is the field operator of electrons. Damping factors of electronic states, Γ, and photons, γ, can emerge in the denominator of Eq. (A1) such as $\omega_{kn}\to\omega_{kn}-i\Gamma_{kn}$ and $\omega_2\to\omega_2+i\gamma_2$, respectively. However, it should be noted here that the compressed expression (A1) with the full permutation operator is available only when such damping factors are additive; $\Gamma_{kn}=\Gamma_{kl}+\Gamma_{ln}$. This is especially true in the infinitesimal-damping limit, $\Gamma_{kn}\to 0$.

Here the low-temperature limit ($\beta\to 0$) is assumed and the many-body states are approximated to single Slater determinants of one-particle Bloch states, $\varphi_{n\mathbf{k}}(\mathbf{x})$, where n is the band index and $\mathbf{k}$ the Bloch wave number. Then the field operator of electrons is expanded in terms of Bloch states such as

$$\hat{\psi}(\mathbf{x})=\sum_{n\mathbf{k}}\hat{C}_{n\mathbf{k}}\varphi_{n\mathbf{k}}(\mathbf{x}),\tag{A3}$$

and each bracket in the numerator of Eq. (A1) is evaluated by separating Bloch states into valence- and conduction-band states. In this case, the sum of many-body states is reduced to the sum of 24 transition processes, each of which is made of four successive one-particle transitions. However, 18 of these processes cancel each other out mathematically because they have the apparent system-size dependence described by the divergent delta functions $\delta(\mathbf{0})$ for wave numbers and physically because each of them is made of noncorrelated one-particle transitions.[49] The remaining six processes are arranged into five terms such as

$$\chi^{(3)}_{abcd}(\mathbf{q}_1,\omega_1;\mathbf{q}_2,\omega_2,\mathbf{q}_3,\omega_3,\mathbf{q}_4,\omega_4) = \frac{1}{|\hat{\mathcal{P}}^{bcd}|}\left(\frac{1}{\hbar}\right)^3\left(\frac{e}{m_0}\right)^4\frac{-1}{\omega_1\omega_2\omega_3\omega_4}\sum_4\sum_3\sum_2\sum_1$$
$$\times\hat{\mathcal{P}}^{abcd}\left\{-\frac{P^a(1^v,4^c)P^c(4^c,3^v)P^b(3^v,2^c)P^d(2^c,1^v)}{[\omega(4^c,1^v)-\omega_2-\omega_3-\omega_4]_\Delta[\omega(4^c,3^v)-\omega_3]_\Delta[\omega(2^c,1^v)-\omega_4]_\Delta}\right.$$
$$+\frac{P^a(1^v,4^c)P^b(4^c,3^c)P^c(3^c,2^c)P^d(2^c,1^v)}{[\omega(4^c,1^v)-\omega_2-\omega_3-\omega_4]_\Delta[\omega(3^c,1^v)-\omega_3-\omega_4]_\Delta[\omega(2^c,1^v)-\omega_4]_\Delta}$$
$$-\frac{P^c(1^v,4^v)P^a(4^v,3^c)P^b(3^c,2^c)P^d(2^c,1^v)}{[\omega(3^c,4^v)-\omega_2-\omega_3-\omega_4]_\Delta[\omega(2^c,4^v)-\omega_3-\omega_4]_\Delta[\omega(2^c,1^v)-\omega_4]_\Delta}$$
$$-\frac{P^d(1^c,2^v)P^b(2^v,3^v)P^a(3^v,4^c)P^c(4^c,1^c)}{[\omega(1^c,2^v)-\omega_4]_\Delta[\omega(4^c,2^v)-\omega_3-\omega_4]_\Delta[\omega(4^c,3^v)-\omega_2-\omega_3-\omega_4]_\Delta}$$
$$\left.+\frac{P^d(1^c,2^v)P^c(2^v,3^v)P^b(3^v,4^v)P^a(4^v,1^c)}{[\omega(1^c,2^v)-\omega_4]_\Delta[\omega(1^c,3^v)-\omega_3-\omega_4]_\Delta[\omega(1^c,4^v)-\omega_2-\omega_3-\omega_4]_\Delta}\right\}, \tag{A4}$$

where

$$\sum_1 \equiv \sum_{n_1}\int\frac{d\mathbf{k}_1}{(2\pi)^3}, \tag{A5}$$

$$P^a(1^v,4^c) \equiv \langle n_1^v\mathbf{k}_1|e^{-i\mathbf{q}_1\mathbf{x}_1}\hat{p}^a|n_4^c\mathbf{k}_4\rangle, \tag{A6}$$

$$\omega(4^c,1^v) \equiv \omega(n_4^c\mathbf{k}_4)-\omega(n_1^v\mathbf{k}_1), \tag{A7}$$

$$\frac{1}{[\omega(4^c,1^v)-\omega_2-\omega_3-\omega_4]_\Delta} \equiv \frac{\Delta(\mathbf{k}_4-\mathbf{k}_1-\mathbf{q}_2-\mathbf{q}_3-\mathbf{q}_4)}{\omega(4^c,1^v)-\omega_2-\omega_3-\omega_4}. \tag{A8}$$

Here we adopt the compressed notation $1 \equiv (n_1,\mathbf{k}_1)$ to display the dependence on the Bloch band state, $|n_1\mathbf{k}_1\rangle \equiv \varphi_{n_1\mathbf{k}_1}(\mathbf{x})$, and its energy, $\omega(n_1\mathbf{k}_1)$. Also 1^c and n_1^c (1^v and n_1^v) indicate that the summation is carried out over only the conduction (valence) bands. Δ is the three-dimensional δ function having the periods of reciprocal-lattice vectors. Note that the $\mathbf{k}$ integration over the Brillouin zone in Eq. (A4) is effectively single because each term in Eq. (A4) has three δ functions with respect to wave numbers, which reflects the fact that four successive one-particle transitions in respective term should be fully correlated to each other. The overall negative sign in three terms in Eq. (A4) comes from the exchange of two electrons. In the literature,[11] the first, the second, and the other terms are sometimes called "three state," "virtual electron," and "virtual hole" processes, respectively.

The imaginary part of $\chi^{(3)}$ represents the energy resonance between the electromagnetic fields and electronic states, and it can be expressed much more compactly by combining five terms in Eq. (A4). For example, the resonant terms with the electromagnetic-field energies, $\omega_2+\omega_3+\omega_4$, $\omega_3+\omega_4$, and ω_4 are

$$\mathrm{Im}\chi^{(3)}_{abcd}(\mathbf{q}_1,\omega_1;\mathbf{q}_2,\omega_2,\mathbf{q}_3,\omega_3,\mathbf{q}_4,\omega_4)$$
$$= \frac{1}{|\hat{\mathcal{P}}^{bcd}|}\left(\frac{1}{\hbar}\right)^3\left(\frac{e}{m_0}\right)^4\frac{-\pi}{\omega_1\omega_2\omega_3\omega_4}\sum_c\sum_v\sum_l\sum_m$$
$$\times\left\{P^a(v,c)\left(\hat{\mathcal{P}}^{bcd}\frac{P^b(c,l)P^c(l,m)P^d(m,v)}{[\omega(l,v)-\omega_3-\omega_4]_\Delta[\omega(m,v)-\omega_4]_\Delta}\right)\delta[\omega(c,v)-\omega_2-\omega_3-\omega_4]_\Delta\right.$$
$$+\left(\hat{\mathcal{P}}^{ab}\frac{P^a(v,l)P^b(l,c)}{[\omega(l,v)-\omega_2-\omega_3-\omega_4]_\Delta}\right)\left(\hat{\mathcal{P}}^{cd}\frac{P^c(c,m)P^d(m,v)}{[\omega(m,v)-\omega_4]_\Delta}\right)\delta[\omega(c,v)-\omega_3-\omega_4]_\Delta$$
$$\left.+\left(\hat{\mathcal{P}}^{abc}\frac{P^a(v,l)P^b(l,m)P^c(m,c)}{[\omega(l,v)-\omega_2-\omega_3-\omega_4]_\Delta[\omega(m,v)-\omega_3-\omega_4]_\Delta}\right)P^d(c,v)\delta[\omega(c,v)-\omega_4]_\Delta+\cdots\right\}, \tag{A9}$$

where

$$\delta[\omega(c,v)-\omega_2-\omega_3-\omega_4]_\Delta \equiv \delta[\omega(c,v)-\omega_2-\omega_3-\omega_4]\Delta(\mathbf{k}_c-\mathbf{k}_v-\mathbf{q}_2-\mathbf{q}_3-\mathbf{q}_4). \tag{A10}$$

Here $c=(n_c,\mathbf{k}_c)$ and $v=(n_v,\mathbf{k}_v)$, respectively, indicate the conduction- and valence-band states, while $l=(n_l,\mathbf{k}_l)$

and $m = (n_m, \mathbf{k}_m)$ are the intermediate states including both the valence and conduction bands.

Two-photon absorption originates from the second term in Eq. (A9). Taking the longwavelength limit, all band-state quantities have the wave number $\mathbf{k}$ as the integral variable. Equation (2.4) in the text is obtained through the replacements such as $P^a(v,l) \rightarrow \langle v\mathbf{k}|\hat{p}^a|l\mathbf{k}\rangle \equiv P^a_{vl}(\mathbf{k})$ and $\omega(l,v) \rightarrow \omega(l\mathbf{k}) - \omega(v\mathbf{k}) \equiv \omega_{lv}(\mathbf{k})$.

[1] R. W. Boyd, *Nonlinear Optics* (Academic, San Diego, 1992).

[2] Y. R. Shen, *The Principles of Nonlinear Optics* (Wiley, New York, 1984).

[3] See, for example, the review paper by V. Nathan, A. H. Guenther, and S. S. Mitra, J. Opt. Soc. Am. B **2**, 294 (1985), and references cited therein.

[4] D. C. Hutchings, M. Sheik-Bahae, D. J. Hagan, and E. W. Van Stryland, Opt. Quantum Electron. **24**, 1 (1992).

[5] M. Sheik-Bahae, D. C. Hutchings, D. J. Hagan, and E. W. Van Stryland, IEEE J. Quantum Electron. **27**, 1296 (1991).

[6] M. Sheik-Bahae, A. A. Said, T. H. Wei, D. J. Hagan, and E. W. Van Stryland, IEEE J. Quantum Electron. **26**, 760 (1990).

[7] B. S. Wherrett, J. Opt. Soc. Am. B **1**, 67 (1984).

[8] D. C. Hutchings and E. W. Van Stryland, J. Opt. Soc. Am. B **9**, 2065 (1992).

[9] D. C. Hutchings and B. S. Wherrett, Phys. Rev. B **49**, 2418 (1994).

[10] D. J. Moss, J. E. Sipe, and H. M. van Driel, Phys. Rev. B **36**, 9708 (1987).

[11] D. J. Moss, E. Ghahramani, J. E. Sipe, and H. M. van Driel, Phys. Rev. B **41**, 1542 (1990).

[12] E. Ghahramani, D. J. Moss, and J. E. Sipe, Phys. Rev. B **43**, 9700 (1991); **43**, 8990 (1991); **43**, 9269 (1991).

[13] Z. H. Levine and D. C. Allan, Phys. Rev. Lett. **63**, 1719 (1989); Phys. Rev. B **43**, 4187 (1991).

[14] Z. H. Levine and D. C. Allan, Phys. Rev. Lett. **66**, 41 (1991); Phys. Rev. B **44**, 12 781 (1991).

[15] M.-Z. Huang and W. Y. Ching, Phys. Rev. B **47**, 9449 (1993); **47**, 9464 (1993); W. Y. Ching and M.-Z. Huang, *ibid.* **47**, 9479 (1993).

[16] A. Vaidyanathan, A. H. Guenther, and S. S. Mitra, Phys. Rev. B **24**, 2259 (1981).

[17] M. Murayama and T. Nakayama, Phys. Rev. B **49**, 5737 (1994).

[18] A. J. Read and R. J. Needs, Phys. Rev. B **44**, 13 071 (1991).

[19] M. Weiler, Solid State Commun. **39**, 937 (1981).

[20] C. C. Lee and H. Y. Fan, Phys. Rev. B **9**, 3502 (1974).

[21] M. Murayama and T. Nakayama, J. Phys. Soc. Jpn. **61**, 2419 (1992).

[22] M. T. Yin and M. L. Cohen, Phys. Rev. B **26**, 5668 (1982).

[23] G. W. Bachelet, D. R. Hamann, and M. Schlüter, Phys. Rev. B **26**, 4199 (1982).

[24] D. Ceperley and B. J. Alder, Phys. Lett. **45**, 566 (1980).

[25] J. P. Perdew and A. Zunger, Phys. Rev. B **23**, 5048 (1981).

[26] J. Ihm, A. Zunger, and M. L. Cohen, J. Phys. C **12**, 4409 (1979).

[27] M. Murayama and T. Nakayama, Phys. Rev. B **49**, 4710 (1994).

[28] *Semiconductors, Physics of Group IV Elements and III-V Compounds*, edited by O. Madelung, Landolt-Börnstein, New Series, Group III, Vol. 17, Pt. a (Springer-Verlag, Berlin, 1982).

[29] *Semiconductors, Physics of II-VI and I-VII Compounds*, edited by O. Madelung, M. Schulz, and H. Weiss, Landolt-Börnstein, New Series, Group III, Vol. 17, Pt. b (Springer-Verlag, Berlin, 1982).

[30] M. S. Hybertsen and S. G. Louie, Phys. Rev. B **34**, 5390 (1986).

[31] R. W. Godby, M. Schlüter, and L. J. Sham, Phys. Rev. B **36**, 6497 (1987); **37**, 10 159 (1988).

[32] G. Lehman and M. Taut, Phys. Status Solidi B **119**, 9 (1983).

[33] C. S. Wang and B. M. Klein, Phys. Rev. B **24**, 3417 (1981).

[34] A. F. Starace, Phys. Rev. A **3**, 1242 (1971).

[35] M. S. Hybertsen and S. G. Louie, Phys. Rev. B **35**, 5585 (1987).

[36] J. L. Freeouf, Phys. Rev. B **7**, 3810 (1973).

[37] The present results without nonlocal corrections are slightly different from those we reported earlier due to the different numerical parameters used in the calculations. Previous calculations were carried out using plane waves with energy less than 14.44 Ry, four conduction bands, and $50 \times 50 \times 50$ $\mathbf{k}$ points for all of Si, ZnSe, and GaAs.

[38] D. H. Reitze, T. R. Zhang, Wm. M. Wood, and M. C. Downer, J. Opt. Soc. Am. B **7**, 84 (1990).

[39] A. A. Said, M. Sheik-Bahae, D. J. Hagan, T. H. Wei, J. Wang, J. Young, and E. W. Van Stryland, J. Opt. Soc. Am. B **9**, 405 (1992).

[40] E. W. Van Stryland, H. Hanherzeele, M. A. Woodall, M. J. Soileau, A. L. Smirl, S. Guha, and T. F. Boggess, Opt. Eng. **24**, 613 (1985).

[41] J. A. Bolger, A. K. Kar, B. S. Wherrett, R. DeSalvo, D. C. Hutchings, and D. J. Hagan, Opt. Commun. **97**, 203 (1993).

[42] A. F. Stewart and M. Bass, Appl. Phys. Lett. **37**, 1040 (1980).

[43] B. Bosacchi, J. S. Bessey, and F. C. Jain, J. Appl. Phys. **49**, 4609 (1978).

[44] Calculations were carried out using plane waves with energy less than 14.44 Ry, scissors-shift energy of 0.12 eV, 20 conduction bands, and $36 \times 36 \times 36$ $\mathbf{k}$ points for zinc-blende ZnS, while using 40 conduction bands and $36 \times 36 \times 18$ $\mathbf{k}$ points for wurtzite ZnS.

[45] M. D. Dvorak, W. A. Schroeder, D. R. Andersen, A. L. Smirl, and B. S. Wherrett, IEEE J. Quantum Electron. **30**, 256 (1994).

[46] J. P. van der Ziel, Phys. Rev. B **16**, 2775 (1977).

[47] R. DeSalvo, M. Sheik-Bahae, A. A. Said, D. J. Hagan, and E. W. Van Stryland, Opt. Lett. **18**, 194 (1993).

[48] J. M. Luttinger and W. Kohn, Phys. Rev. **97**, 869 (1955).

[49] H. Ishihara and K. Cho, Phys. Rev. B **42**, 1724 (1990).